J Biol Inorg Chem (2007) 12:406–420
DOI 10.1007/s00775-006-0197-3

ORIGINAL PAPER

Physicochemical and MRI characterization of Gd^{3+}-loaded polyamidoamine and hyperbranched dendrimers

Zoltán Jászberényi · Loïck Moriggi · Philipp Schmidt · Claudia Weidensteiner · Rainer Kneuer · André E. Merbach · Lothar Helm · Éva Tóth

Received: 19 October 2006 / Accepted: 24 November 2006 / Published online: 10 January 2007

Abstract Generation 4 polyamidoamine (PAMAM) and, for the first time, hyperbranched poly(ethylene imine) or polyglycerol dendrimers have been loaded with Gd^{3+} chelates, and the macromolecular adducts have been studied in vitro and in vivo with regard to MRI contrast agent applications. The Gd^{3+} chelator was either a tetraazatetracarboxylate DOTA-*p*Bn^{4-} or a tetraazatricarboxylate monoamide DO3A-MA^{3-} unit. The water exchange rate was determined from a ^{17}O NMR and ^{1}H Nuclear Magnetic Relaxation Dispersion study for the corresponding monomer analogues [Gd(DO3A-AEM)(H_2O)] and [Gd(DOTA-*p*Bn-NH_2)(H_2O)]$^-$ (k_{ex}^{298} = 3.4 and 6.6×10^6 s^{-1}, respectively), where H_3DO3A-AEM is {4-[(2-acetylaminoethylcarbamoyl)methyl]-7,10-bis(carboxymethyl-1,4,7,10-tetraazacyclododec-1-yl)}-acetic acid and H_4DOTA-*p*Bn-NH_2 is 2-(4-aminobenzyl)-1,4,7,10-tetraazacyclododecane-1,4,7,10-tetraacetic acid. For the macromolecular complexes, variable-field proton relaxivities have been measured and analyzed in terms of local and global motional dynamics by using the Lipari–Szabo approach. At frequencies below 100 MHz, the proton relaxivities are twice as high for the dendrimers loaded with the negatively charged Gd(DOTA-*p*Bn)$^-$ in comparison with the analogous molecule bearing the neutral Gd(DO3A-MA). We explained this difference by the different rotational dynamics: the much slower motion of Gd(DOTA-*p*Bn)$^-$-loaded dendrimers is likely related to the negative charge of the chelate which creates more rigidity and increases the overall size of the macromolecule compared with dendrimers loaded with the neutral Gd(DO3A-MA). Attachment of poly(ethylene glycol) chains to the dendrimers does not influence relaxivity. Both hyperbranched structures were found to be as good scaffolds as regular PAMAM dendrimers in terms of the proton relaxivity of the Gd^{3+} complexes. The in vivo MRI studies on tumor-bearing mice at 4.7 T proved that all dendrimeric complexes are suitable for angiography and for the study of vasculature parameters like blood volume and permeability of tumor vessels.

Keywords MRI contrast agents · Dendrimers · Hyperbranched · Gadolinium · Rotational dynamics

Abbreviations

CA	Contrast agent
DCE	Dynamic contrast enhanced
DTPA	Diethylenetriamin-pentaacetic acid
EPR	Electron paramagnetic resonance
FLASH	Fast low-angle shot
FOV	Field of view

Electronic supplementary material The online version of this article (doi:10.1007/s00775-006-0197-3) contains supplementary material, which is available to authorized users.

Z. Jászberényi · L. Moriggi · A. E. Merbach · L. Helm · É. Tóth
Institut des Sciences et Ingénierie Chimiques, Ecole Polytechnique Fédérale de Lausanne, ISIC, BCH, 1015 Lausanne, Switzerland

P. Schmidt · C. Weidensteiner · R. Kneuer
Novartis Institutes for Biomedical Research, Novartis Pharma AG, 4002 Basel, Switzerland

É. Tóth (✉)
Centre de Biophysique Moléculaire, CNRS, rue Charles Sadron, 45071 Orléans, France
e-mail: eva.jakabtoth@cnrs-orleans.fr

G4	Generation 4
H_3DO3A-AEM	{4-[(2-Acetylaminoethylcarbamoyl)methyl]-7,10-bis(carboxymethyl-1,4,7,10-tetraazacyclododec-1-yl)}-acetic acid
H_4DOTA-*p*Bn-NH_2	2-(4-Aminobenzyl)-1,4,7,10-tetraazacyclododecane-1,4,7,10-tetraacetic acid
H_4DOTA-*p*Bn-SCN is	2-(4-Isothiocyanatobenzyl)-1,4,7,10-tetraazacyclododecane-1,4,7,10-tetraacetic acid
H_4DOTA-NHS	1,4,7,10-Tetraazacyclododecane-1,4,7,10-tetraacetic acid mono(*N*-hydroxysuccinimide ester)
HB	Hyperbranched
HEPES	*N*-(2-Hydroxyethyl)piperazine-*N*′-ethanesulfonic acid
ICP	Inductively coupled plasma
IR	Inversion recovery
MA	Monoamide
mPEG-SPA	Methoxypoly(ethylene glycol)–succinimidyl propionate
MRI	Magnetic resonance imaging
NMRD	Nuclear Magnetic Relaxation Dispersion
PAMAM	Polyamidoamine
PEG	Poly(ethylene glycol)
PEI	Poly(ethylene imine)
PG	Polyglycerol
RARE	Rapid acquisition and relaxation enhancement, fast spin echo MRI method
ROI	Region of interest
TE	Echo time
TR	Repetition time
ZFS	Zero-field splitting

Introduction

Magnetic resonance imaging (MRI) is one of the most performant modalities in current clinical diagnostics which provides noninvasive, high-resolution in vivo mapping of body tissues. Magnetic resonance images are based on the NMR signals of protons, mainly those of water. Image contrast is created by differences in signal intensity and allows for discrimination between various tissues [1]. The contrast can be achieved in different ways: based on different water content in the tissues or by weighting the imaging sequence to display differences in proton relaxation rates ($1/T_1$ or $1/T_2$), chemical shifts, water diffusion, or blood flow. In T_1-weighted imaging, faster longitudinal relaxation is associated with higher signal intensity. The longitudinal relaxation rate of water protons can be enhanced by application of paramagnetic compounds, called contrast agents (CAs), which provide increased image contrast in regions where the paramagnetic agent localizes [2, 3].

Relaxivity is the ability of paramagnetic compounds to increase the relaxation rates of the surrounding water proton spins, by definition referred to unit concentration of the paramagnetic center (millimoles per liter). Given its high magnetic moment and relatively slow electron spin relaxation, Gd^{3+} is particularly adapted to CA applications. Indeed, beside iron oxide nanoparticles, stable Gd^{3+} chelates are widely used in clinical practice. The paramagnetic relaxation effect originates from two distinct mechanisms: the inner-sphere relaxation term is related to short-distance interactions between the paramagnetic metal ion and the water protons in the inner coordination sphere, while the outer-sphere relaxation term is the result of long-distance interactions between the metal ion and water protons diffusing in the proximity of the complex. The main factors determining the inner-sphere relaxivity are the number of coordinated water molecules and their exchange rate, the rotational dynamics of the complex, and the relaxation times of the Gd^{3+} electron spin. The outer-sphere term is related to the diffusion of the complex, to the closest distance of approach between bulk water molecules and the Gd^{3+}, and to the electron spin relaxation.

For years now, macromolecular compounds have been extensively explored as potential MRI CAs. The macromolecular nature results in both positive and negative aspects with regard to a possible biological application. Macromolecules will have increased rotational correlation time, contributing to an enhanced relaxivity. Moreover, attachment of a large number of paramagnetic chelates to one macromolecular entity will increase the local concentration of Gd^{3+} and consequently a lower injected dose may be sufficient for image acquisition. On the other hand, macromolecules have a longer blood pool retention time, which may represent an increased risk to the patient. Various classes of macromolecular CAs, including dendrimers, have shown very interesting features in biomedical applications and this prompted

their detailed physicochemical and biological characterization.

Dendrimers are large molecules with well-defined chemical structures, with a regular and highly branched three-dimensional scaffold. Unlike classic polymers, dendrimers have a high degree of molecular uniformity, narrow molecular weight distribution, specific size characteristics, and a highly functionalized surface. They consist of three major architectural components: core, branches, and end groups. Polymerization of dendrimers is a process using a series of repetitive steps starting with the central initiator core. Each subsequent step represents a new ''generation'' of the polymer with a larger molecular diameter, doubles in general the number of reactive surface sites, and approximately doubles the molecular weight from that of the preceding generation. One of the most interesting aspects of the technologies based on dendrimers is that they may be tailored for specific purposes and with specific functionality for a variety of applications involving the pharmaceutical and biomedical area [4–6]. The molecules can be designed to pass into cells and can be used to deliver substances such as drugs, genetic material, or chemical markers right into the cell. Gd^{3+} complexes attached to dendrimers have already been investigated in the context of MRI CA applications [7–13].

Polyamidoamine (PAMAM) dendrimers represent a specific class with interesting characteristics and potential for biomedical applications [14, 15]. They are synthesized by Michael addition of methyl acrylate to an amine core. High-generation PAMAM dendrimers are generally accepted to be spherical molecules, with the core and interior being almost completely shielded owing to the numerous terminal surface groups. The molecular size and the number of the terminal groups of PAMAM dendrimers were found to largely affect their biodistribution.

Hyperbranched (HB) structures are similar to dendrimers, but they are prepared in a random one-pot synthesis from monomers having branching potential, with low control over structure and molar mass. Their architecture is less precisely defined; some branches are missing, there are more holes in the structure and fewer active chemical groups at the surface of the molecule. HB polymers have become by now an established class of polymeric materials and can be considered as highly functional specialty products [16]. By modification of the end groups, the properties of HB polymers can significantly change, leading to diverse possible applications. Polyglycerol (PG) is a water-soluble polymer that contains ether linkages. The low cytotoxicity and the FDA approval as emulsifiers in the pharmaceutical and food industries make it a particularly promising polymer for use in the biomedical field [17].

Here we report the synthesis and in vitro and in vivo characterization of a series of PAMAM and, for the first time, HB dendrimeric structures loaded with various Gd^{3+} chelates on their surface. The following compounds were investigated with regard to MRI CA applications: a generation 4 (G4) PAMAM dendrimer loaded with GdDO3A monoamide (MA) complexes (PAMAM-G4-[Gd(DO3A-MA)$(H_2O)]_{31}$), or with Gd(DOTA)$^-$ (PAMAM-G4-[Gd(DOTA-*p*Bn)$(H_2O)]^-_{33}$), its PEGylated [PEG is poly(ethylene glycol)] derivative (PAMAM-G4-PEG-[Gd(DOTA-*p*Bn)$(H_2O)]^-_{38}$), a HB poly(ethylene imine) (PEI) based polymer (HB-PEI-[Gd(DOTA-*p*Bn)$(H_2O)]^-_{32}$), and a HB PG-based molecule (HB-PG-[Gd(DOTA-*p*Bn)$(H_2O)]^-_{68}$; Scheme 1). ^{1}H Nuclear Magnetic Relaxation Dispersion (NMRD) measurements were performed on the compounds and their rotational dynamics has been described by analyzing the proton relaxivities with the Lipari–Szabo approach in terms of global and local motions [18, 19]. In addition to the macromolecular chelates, the corresponding monomer Gd^{3+} complexes of the surface chelators, [Gd(DO3A-AEM)(H_2O)] and [Gd(DOTA-*p*Bn-NH_2)$(H_2O)]^-$, were the subject of a variable-temperature ^{17}O NMR and ^{1}H relaxivity investigation (Scheme 2) which allowed the assessment of their water exchange and rotational dynamics (H_3DO3A-AEM is {4-[(2-acetylaminoethylcarbamoyl) methyl]-7,10-bis(carboxymethyl-1,4,7,10-tetraazacyclo dodec-1-yl)}-acetic acid; H_4DOTA-*p*Bn-NH_2 is 2-(4-aminobenzyl)-1,4,7,10-tetraazacyclododecane-1,4,7,10-tetraacetic acid).

Considerably different proton relaxivities have previously been reported for PAMAM dendrimers loaded with DOTA and DO3A-MA type chelators [8, 9], and this difference was also confirmed in our study. A specific objective of the present work was to rationalize this divergence. In addition, we also compared the effect of the internal structure of the dendrimers (regular PAMAM or HB) on the proton relaxivities. Altogether, the series of macromolecules studied here allowed us to systematically explore how the relaxivities are affected (1) by the variation of the chelating unit [negatively charged Gd(DOTA-*p*Bn)$^-$ or neutral Gd(DO3A-MA)], (2) by the dendrimer surface (PEGylated or not), and (3) by the regular dendrimeric or HB nature of the macromolecule. The in vitro physicochemical characterization of these macromolecular systems was completed by in vivo MRI studies in tumor-bearing mice in order to evaluate their efficacy for biological studies.

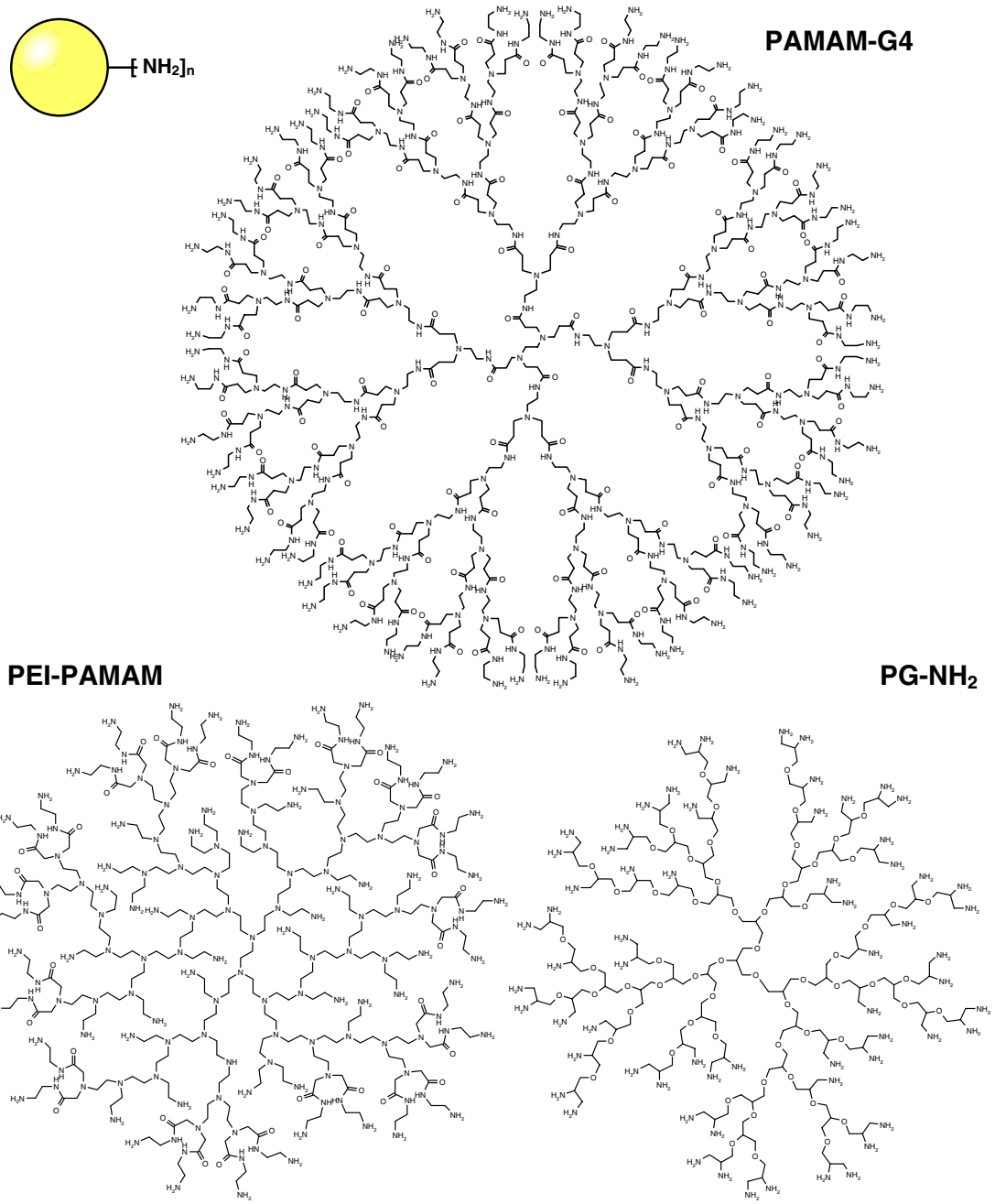

Scheme 1 Different dendrimers as macromolecular scaffolds for MRI contrast agents: ethylenediamine-cored polyamidoamine, generation 4 (*PAMAM-G4*) (*top*); hyperbranched, ethylenediamine-cored poly(ethylene imine) (*PEI*) (*bottom left*); hyperbranched, amino-functionalized polyglycerol ($PG\text{-}NH_2$) (*bottom right*)

Scheme 2 Different moieties attached to the respective dendrimers via amide or thiourea bonds

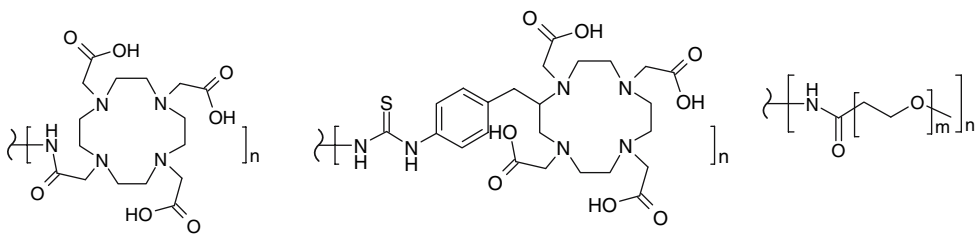

– DO3A-MA **–DOTA-*p*Bn** **– mPEG**

Materials and methods

PAMAM-G4 dendrimer, ethylenediamine core, was purchased from Dendritech, Midland, MI, USA. PEI-PAMAM [20] (PEI core M_w = 6,000, 6.2 nmol NH_2 g^{-1}) and amino-functionalized PG [21] (PG core M_w = 8,000, 13.6 nmol NH_2 g^{-1}) HB dendrimers were obtained from Rainer Haag, Freie Universität Berlin, Germany. The bifunctional chelating agents DOTA-*p*Bn-SCN [H_4DOTA-*p*Bn-SCN is 2-(4-isothiocyanatobenzyl)-1,4,7,10-tetraazacyclododecane-1,4,7,10-tetraacetic acid], DOTA-*p*Bn-NH_2, and DOTA-NHS [H_4DOTA-NHS is 1,4,7,10-tetraazacyclododecane-1,4,7,10-tetraacetic acid mono(*N*-hydroxysuccinimide ester)] were purchased from Macrocyclics, TX, USA. Gadolinium chloride hexahydrate was purchased from Sigma-Aldrich, Buchs, Switzerland. Ultrafiltration membranes were purchased from Millipore, Bedford, MA, USA. Methoxypoly(ethylene glycol)–succinimidyl propionate (mPEG-SPA; M_W = 5,000) was purchased from Nektar Therapeutics, San Carlos, CA, USA.

Elemental analyses were performed by Solvias, Basel, Switzerland, and mass spectrometry was performed with a MAT 900 double-sector mass spectrometer.

Synthesis of H_3DO3A-AEM

DOTA-NHS and *N*-acetylethylendiamine were dissolved in dimethylformamide (Scheme 3). After addition of *N*-ethyldiisopropylamine, the reaction mixture was stirred for 2 h at room temperature. The product was purified by column chromatography (SiO_2, ethyl acetate/methanol 2/1).

^{1}H NMR (400 MHz, D_2O, δ): 1.89 (s, 3 H), 2.87–2.96 (m, 4 H), 2.99–3.07 (m, 4 H), 3.16–3.24 (m, 4 H), 3.28–3.49 (m, 10 H), 3.36 (d, J = 4.2 Hz, 2 H), 3.7 (m, 4 H); ^{13}C NMR (101 MHz, D_2O, δ): 22.0, 36.8, 38.5, 38.5, 39.2, 48.2, 48.3, 50.6, 51.7, 54.5, 56.0, 56.4, 169.8, 172.3, 174.4, 176.2, 176.3. MS m/z: 529.8 $[M + H]^+$.

Synthesis of the dendrimers

The respective dendrimer was dissolved in $NaHCO_3$ solution (0.1 M) and adjusted to pH 9 by Na_2CO_3 solution (1 M) if necessary. The same procedure was carried out for DOTA-*p*Bn-SCN or DOTA-NHS (1.2 equiv of all free dendrimer amino sites) and after combining both solutions the reaction mixture was stirred for 18 h at room temperature (pH control). At this point the PEGylated dendrimer can be synthesized by adding mPEG-SPA to the reaction mixture and with additional stirring for 2 h at room temperature. Purification was done by ultrafiltration (SFCA, molecular weight cutoff 10,000: five times $NaHCO_3$ solution (0.1 M); five times double-distilled water). The chelate-to-dendrimer ratio (Table 1) was determined by ^{1}H NMR (e.g., correlating the four aromatic proton signals of DOTA-*p*Bn or –CH_2– of the MA unit in DO3A-MA and –CH_2–CONH– of the G4 dendrimer). The loading of the PAMAM dendrimers with the macrocyclic ligand was between 60 and 70% with respect to the overall number of terminal amines (64 for PAMAM-G4 with an ethylenediamine core). The degree of PEGylation could also be correlated by ^{1}H NMR (–CH_2–CH_2–O– repeating unit).

Gd^{3+} loading on the dendrimers

After gadolinium chloride had been dissolved in citrate buffer (0.1 M, pH 5) and the pH had been adjusted to 8 by NaOH (1 M), the solution and the dendrimer dissolved in citrate buffer were combined and stirred for 48 h at room temperature. Ultrafiltration (SFCA, molecular weight cuttoff 10,000: five times citrate buffer (0.1 M, pH 8); five times double-distilled water) was continued until the eluant tested negative for free Gd^{3+} (xylenol orange test, acetate buffer, pH 6). Lyophilization gave cotton-like solids. Inductively coupled plasma (ICP) spectroscopy was used to determine the Gd^{3+} content.

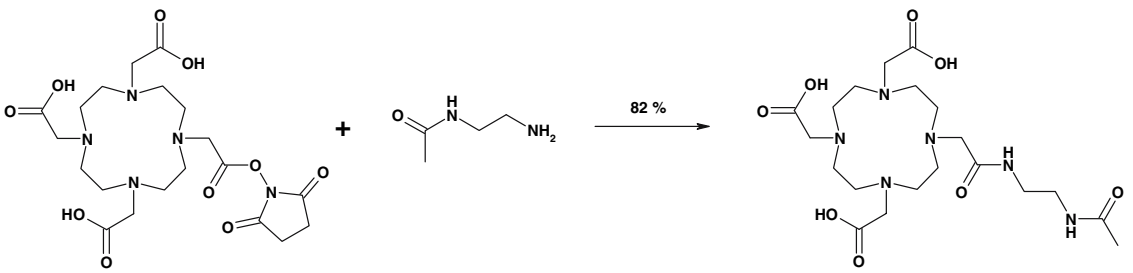

Scheme 3 Synthesis of {4-[(2-acetylaminoethylcarbamoyl)methyl]-7,10-bis(carboxymethyl-1,4,7,10-tetraazacyclododec-1-yl)}-acetic acid

Table 1 Analytical data of the dendrimers studied

Dendrimer	Chelate-to-dendrimer ratio (NMR)	Gd content (ICP-OES) (%)	Gd per gram dendrimer (mmol)	Gd/dendrimer (calc.)	Molecular mass (calc.) (kDa)
PAMAM-G4-[Gd(DOTA-*p*Bn)(H_2O)]$^{-}_{33}$	45	11.6	0.738	33	45
PAMAM-G4-[Gd(DO3A-MA)(H_2O)]$_{31}$	38	14.1	0.897	31	35
PAMAM-G4-PEG-[Gd(DOTA-*p*Bn)(H_2O)]$^{-}_{38}$[a]	40	10.0	0.636	38	60
HB-PEI-[Gd(DOTA-*p*Bn)(H_2O)]$^{-}_{32}$	39	10.2	0.649	32	50
HB-PG-[Gd(DOTA-*p*Bn)(H_2O)]$^{-}_{68}$	93	11.3	0.719	68	95

For an explanation of the dendrimer nomenclature, see the text

ICP-OES inductively coupled plasma optical emission spectroscopy

[a] 4× PEG/dendrimer

Preparation of the samples

Solutions of the monomer GdL complexes were prepared by mixing equimolar amounts of $Gd(ClO_4)_3$ and the ligand. A slight excess of ligand (5%) was used and the pH was adjusted to about 5–6 by adding 0.1 M $HClO_4$ or 0.1 M NaOH. In each sample the absence of free metal was checked by the xylenol orange test. $Gd(ClO_4)_3$ stock solution was prepared by dissolving Gd_2O_3 (Sigma-Aldrich) in a slight excess of $HClO_4$ (Merck p.a. 60%) in double-distilled water. Its concentration was determined by complexometric titration with standardized Na_2H_2EDTA solution using xylenol orange as the indicator.

To improve sensitivity in the ^{17}O NMR samples ^{17}O-enriched water (Izotec, ^{17}O 11.4%) was used (final enrichment approximately 1–2%) and the pH was checked again. The concentration and pH of the samples were as follows: [Gd(DOTA-*p*Bn-NH_2)(H_2O)]$^{-}$ 4.444×10^{-2} mol kg^{-1}, pH 5.64 (^{17}O NMR), 1.223×10^{-2} M, pH 5.53 (NMRD); [Gd(DO3A-AEM)(H_2O)] 4.145×10^{-2} mol kg^{-1}, pH 5.28 (^{17}O NMR), 4.290×10^{-3} M, pH 5.37 (NMRD).

In the case of dendrimers, the NMRD measurements were performed at physiological pH using *N*-(2-hydroxyethyl)piperazine-*N*′-ethanesulfonic acid (HEPES) buffer. In each sample, the Gd^{3+} ion and HEPES buffer concentrations were 1 mM and 0.05 M, respectively and the pH was around 7.4. The concentration of the Gd^{3+} ion was checked by ICP atomic emission spectroscopy for each sample.

^{17}O NMR measurements

At different temperatures from 275 to 366 K, longitudinal and transverse ^{17}O relaxation rates and chemical shifts were measured. The measurements were performed using a Bruker ARX-400 (9.4-T, 54.2-MHz) spectrometer. In order to maintain constant temperature, a Bruker BVT-3000 temperature-control unit was used, with the temperature being measured by a substitution technique [22]. The samples were sealed in glass spheres, adapted to 10-mm NMR tubes, to eliminate susceptibility corrections to the chemical shifts [23]. As an external reference, an aqueous $HClO_4$ solution (pH 3.0) was used. Longitudinal relaxation rates, $1/T_1$, were measured by the inversion-recovery (IR) method and transverse relaxation rates, $1/T_2$, were obtained by the Carr–Purcell–Meiboom–Gill spin-echo technique.

Nuclear Magnetic Relaxation Dispersion

The measurements of NMRD profiles were performed at 298 and 310 K using a Stelar Spinmaster FFC fast field cycling NMR relaxometer equipped with a VTC90 temperature-control unit (Stelar, Italy) (2×10^{-4}—0.47 T, corresponding to ^1H Larmor frequencies from 0.01 to 20 MHz). At higher fields, ^1H $1/T_1$ values were measured with Bruker Minispecs mq30 (30 MHz), mq40 (40 MHz), and mq60 (60 MHz) and with 1.18-T (50-MHz), 2.35-T (100-MHz), and 4.70-T (200-MHz) cryomagnets connected to a Bruker Avance-200 console. The temperature was measured by a substitution technique in each case [22].

Data analysis

The least-squares fits of the ^{17}O NMR and NMRD data were performed by Visualiseur/Optimiseur programs working on a Matlab platform [24, 25]. The reported errors correspond to one standard deviation obtained by the statistical analysis.

MRI sequence

Magnetic resonance measurements were performed with a 4.7-T Bruker Biospec magnetic resonance system (Bruker Biospin, Ettlingen, Germany) equipped with a 12-cm-bore gradient system using a birdcage resonator with inner diameter of 35 mm.

For anatomical reference, a multislice rapid acquisition and relaxation enhancement (RARE) sequence (a fast spin-echo MRI method) was performed with the following parameters: RARE factor 16, echo time (TE) 10 ms, relaxation time (TR) 2.5 s, 15 axial slices, slice thickness 1.5 mm, field of view (FOV) 3.3 cm × 3.3 cm, matrix 256 × 128. Regional CA uptake was assessed with dynamic contrast enhanced (DCE) MRI as follows. A series of IR fast low-angle shot (FLASH) images (a fast gradient-echo MRI method with inversion prepulse [26]) were acquired using the following parameters: TE 3.0 ms, TR 6.9 ms, one axial slice, slice thickness 1.5 mm, FOV 4.1 cm × 4.1 cm, matrix 128 × 96, inversion delay 1.2 s, 128 repetitions with temporal resolution 6 s, duration 12 min. CA was injected at repetition 8 (see below). Before the start of the DCE-MRI series, a reference image was acquired with the same sequence parameters but without the inversion pulse. Additionally, coronal IR FLASH images were acquired with the same imaging parameters before and after the IR FLASH series.

Animal preparation

All studies described in this report were performed in strict adherence to the Swiss law for animal protection.

RIF-1 tumor cells (murine radiation-induced fibrosarcoma) were injected subcutaneously (5×10^6 cells per mouse) in the lower flank of anaesthetized female C3H/He mice (n = 3, 20–25 g, obtained from Charles River Laboratories France). Magnetic resonance experiments started after 3 weeks of growth when the tumor diameter was approximately 1 cm. The animals were anaesthetized with isoflurane (1.5–2.5%) in an O_2/N_2O 1:2 mixture applied with a face mask allowing free breathing. The temperature was kept at 311 K with a current of warm air, and the respiration was monitored. PAMAM-G4-PEG-[Gd(DOTA-pBn)$(H_2O)]^-_{38}$ (1.32 μmol kg^{-1} body weight) was injected as a bolus via a tail vein catheter with an infusion pump (3 ml min^{-1}). A 5 μl g^{-1} body weight aliquot of the CA solution was injected. This corresponded to a dose of 0.05 mmol Gd kg^{-1} body weight.

MRI data processing

The CA concentration was calculated from the change in signal intensity S in the DCE-MRI series with software tools developed in-house. T_1 maps were calculated on a pixel-by-pixel basis from each image using the standard IR equation [27]:

$$T_1 = \frac{-\mathrm{TI}}{\ln\left(0.5\left(1 - \frac{S}{S_0}\right)\right)}, \quad (1)$$

where TI is the inversion time and S_0 is the signal intensity in the precontrast reference image. Maps of the CA concentration C_m were then calculated with following formula

$$C_m = \frac{\frac{1}{T_1} - \frac{1}{T_{10}}}{r_1} \quad (2)$$

using the relaxivity r_1 for PAMAM-G4-PEG-[Gd(DOTA-pBn)$(H_2O)]^-_{38}$ of 8.22 s^{-1} mM^{-1} at 4.7 T and 310 K (Table S8). T_{10} was the mean baseline T_1, i.e., the mean of the first seven scans.

Mean CA concentration time courses $C_m(t)$ were calculated in several regions of interests (ROIs): paravertebral muscle, kidney cortex, kidney medulla, tumor rim, tumor core, and blood pool in the vena cava.

Results and discussion

Synthesis of the ligands and the dendrimers

All monomeric Gd^{3+} chelators were commercially available, except H_3DO3A-AEM. The latter macrocycle was synthesized by addition of *N*-acetylethylenediamine to the activated DOTA-NHS ester, followed by chromatography purification (Scheme 3).

The dendrimeric CAs were synthesized by addition of the respective macrocyclic precursor to the dendrimer under basic conditions. After workup by ultrafiltration, the chelate attachment could be quantified by ^{1}H NMR. For subsequent studies, a PAMAM-G4 dendrimer was labeled by PEG chains on free amino groups via mPEG-SPA to extend the blood half life of the dendrimer [28]. Owing to a longer vascular circulation, PEGylated dendrimers as carriers for target specific CAs were assumed to have a better opportunity to bind to endothelial receptors in the following studies. Addition of PEG chains followed the same procedure as that of the chelators, since aqueous reactions at around pH 9 showed the best conversion rates and yields. Gadolinium loading took place in the last step in citrate buffer at pH 8 for optimal complexation, and it was then assessed by elemental analysis.

^{17}O NMR and NMRD measurements on the monomeric Gd^{3+} complexes

In order to determine the water exchange rate, a variable-temperature ^{17}O NMR study was performed on

aqueous solutions of $[Gd(DOTA\text{-}p\text{Bn-}NH_2)(H_2O)]^-$ and $[Gd(DO3A\text{-}AEM)(H_2O)]$, which represent the monomeric Gd^{3+} complex analogues of the dendrimeric systems investigated. Proton NMRD profiles of these Gd^{3+} complexes were also measured at two temperatures in order to determine parameters that describe rotation and electronic relaxation. For a given Gd^{3+} complex, all experimental data, i.e., the longitudinal ($1/T_{1r}$) and transverse ($1/T_{2r}$) relaxation rates, the ^{17}O chemical shifts ($\Delta\omega_r$), and the longitudinal proton relaxivities (r_1), were analyzed simultaneously using the Solomon–Bloembergen–Morgan equations [29] (see electronic supplementary material). In accordance with previously reported, analogous Gd^{3+}-DOTA and Gd^{3+}-DO3A-MA type derivatives, for both Gd^{3+} complexes we assumed one inner-sphere water molecule (q). The ^{17}O scalar coupling constants, $A/\hbar$, calculated for the complexes in this way are in the usual range observed for Gd^{3+} complexes, which justifies the assumption of $q = 1$. The experimental ^{17}O NMR and NMRD data and the fitted curves for both complexes are shown in Fig. 1. The most relevant parameters obtained in the simultaneous fit are given in Table 2 and the others are given in the electronic supplementary material.

At lower temperatures, the transverse ^{17}O relaxation rates, $1/T_{2r}$, increase with increasing temperature, indicating that the systems are in the slow-exchange regime for both $[Gd(DOTA\text{-}p\text{Bn-}NH_2)(H_2O)]^-$ and $[Gd(DO3A\text{-}AEM)(H_2O)]$. Here $1/T_{2r}$ is determined by the water exchange rate, k_{ex}, and the electronic relaxation does not contribute to the experimental ^{17}O relaxation rates; therefore, even in the absence of electron paramagnetic resonance (EPR) measurements, the water exchange rate can be determined with good accuracy. The Solomon–Bloembergen–Morgan theory uses only the transient contribution to the zero-field splitting (ZFS) to describe electron spin relaxation and discards the static contribution to ZFS [30, 31]. The correlation time as well as the ZFS amplitude obtained can, however, be considered as ''effective'' values τ_{eff} and Δ_{eff}^2 [32]. The values obtained for the monomeric complexes studied here are in agreement with previous results for small Gd^{3+} complexes (see electronic supplementary material) [33].

The values of the rotational correlation time obtained from the simultaneous analysis of ^{17}O and ^1H longitudinal relaxation rates for $[Gd(DOTA\text{-}p\text{Bn-}NH_2)(H_2O)]^-$ and $[Gd(DO3A\text{-}AEM)(H_2O)]$ are also in the usual range expected for low molecular weight Gd^{3+} complexes (Table 2).

Water exchange rates of the monomeric Gd^{3+} complexes

The water exchange rate obtained for $[Gd(DOTA\text{-}p\text{Bn-}NH_2)(H_2O)]^-$ is higher, while that of $[Gd(DO3A\text{-}AEM)(H_2O)]$ is lower than k_{ex} for the parent complex $[Gd(DOTA)(H_2O)]^-$ (Table 2). According to the literature, C-substitution on the ethylenediamine bridge of acyclic diethylenetriaminepentaacetic acid (DTPA) derivatives [34–36] or on the tetraazacyclododecane ring of macrocyclic DOTA-type Gd^{3+} complexes [37] decreases the residence time of the coordinated water molecule, and thus increases the water exchange rate, and was explained by conformational or steric effects. The value of $6.6 \times 10^6\ s^{-1}$ for $[Gd(DOTA\text{-}p\text{Bn-}NH_2)(H_2O)]^-$ as compared with $4.6 \times 10^6\ s^{-1}$ for $[Gd(DOTA)(H_2O)]^-$ follows this observation. On the other hand, for all amide derivatives both in the DTPA and in the DOTA family a decrease of the water exchange rate has been observed [29]. This decrease was explained by two factors: (1) a less negative charge and (2) a decreased steric crowding around the water binding site in the amides in comparison to the carboxylate complexes. Gd^{3+} poly(amino carboxylate) complexes usually undergo a dissociative or a dissociative interchange (I_d) water exchange process. The charge of the complex is of major importance in dissociative processes: a higher negative charge helps the coordinated water molecule to leave and therefore increases the rate of exchange. The role of the steric crowding around the water binding site is also relevant; e.g., an increase in k_{ex} of 2 orders of magnitude could be achieved for the Gd^{3+} complex by elongating the amine backbone of $DTPA^{5-}$ or $DOTA^{4-}$ [38]. The amide oxygen is less strongly bound to the metal than the carboxylate oxygen; therefore, the steric crowding is less important and this will again contribute to slowing down the water exchange as also observed in our case.

Proton relaxivities of the macromolecular Gd^{3+} complexes

Water proton relaxivities were measured at two different temperatures (298 and 310 K) as a function of the Larmor frequency for PAMAM-G4–$[Gd(DOTA\text{-}p\text{Bn})(H_2O)]^-_{33}$, PAMAM-G4–$[Gd(DO3A\text{-}MA)(H_2O)]_{31}$, PAMAM-G4–PEG-$[Gd(DOTA\text{-}p\text{Bn})(H_2O)]^-_{38}$, and HB HB-PEI-$[Gd(DOTA\text{-}p\text{Bn})(H_2O)]^-_{32}$, and HB-PG-$[Gd(DOTA\text{-}p\text{Bn})(H_2O)]^-_{68}$. As expected for slowly rotating macromolecules, a relaxivity hump in the ^1H NMRD profile is observed between 3 and 200 MHz for each system (Fig. 2). However, very different relaxivity

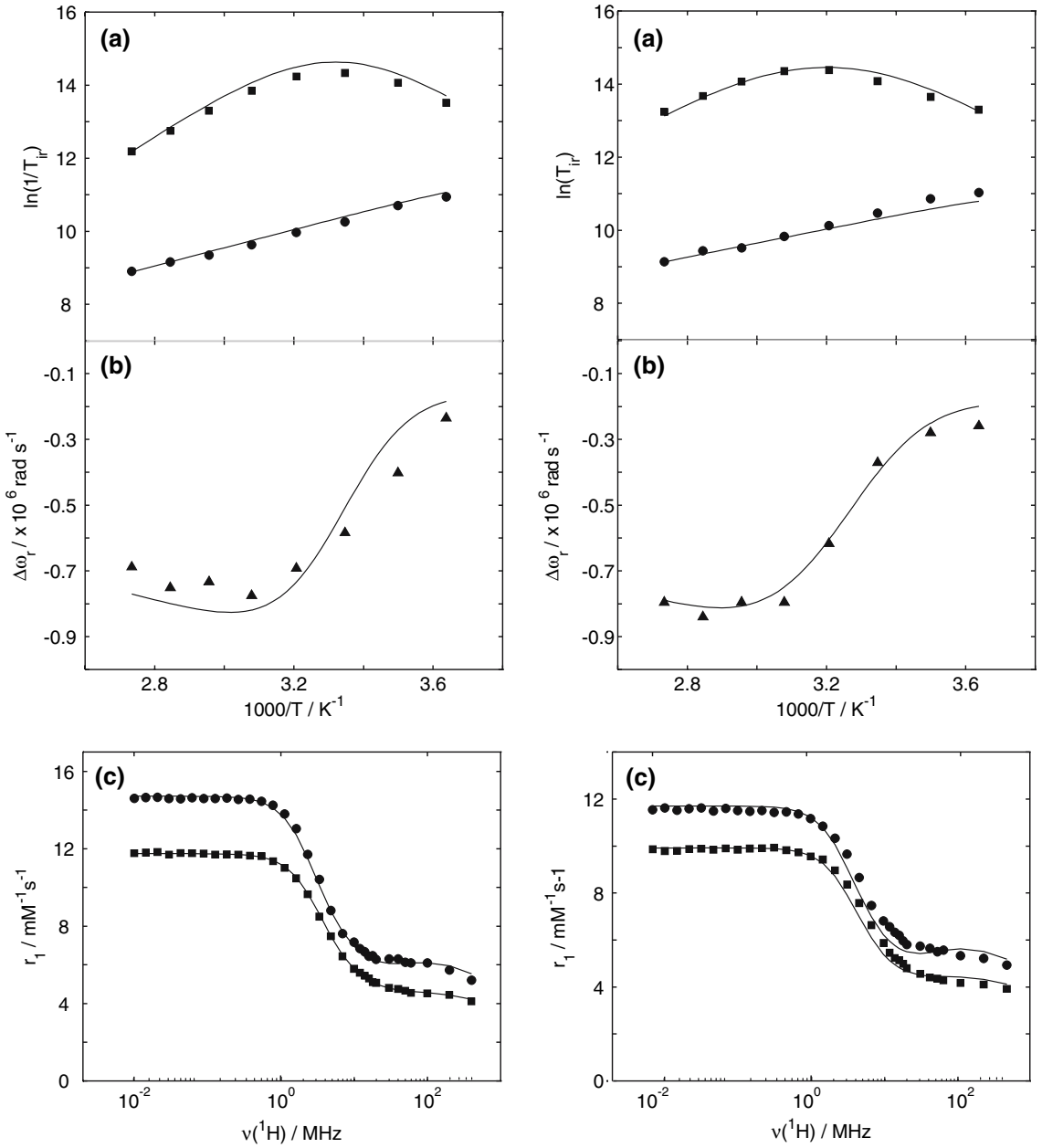

Fig. 1 Temperature dependence of reduced ^{17}O transverse (*squares*) and longitudinal (*circles*) relaxation rates (*a*), reduced chemical shifts (*triangles*) at 9.4 T (*b*), and ^{1}H NMR dispersion (*NMRD*) profiles at 298 K (*circles*) and 310 K (*squares*) (*c*) for $[Gd(DOTA\text{-}p\text{Bn-}NH_2)(H_2O)]^-$ (*left*) and [Gd(DO3A-AEM)(H_2O)] (*right*). The *lines* represent the curves fitted to the experimental data points

values are obtained for the PAMAM-G4 dendrimers when they are loaded with DOTA or DO3A amide chelators (Fig. 2, panels a, b). The PAMAM-G4-$[Gd(DOTA\text{-}p\text{Bn})(H_2O)]^-_{33}$ and PAMAM-G4-PEG-$[Gd(DOTA\text{-}p\text{Bn})(H_2O)]^-_{38}$ dendrimers containing a tetracarboxylate DOTA chelating unit have approximately double ^{1}H relaxivities at Larmor frequencies below 200 MHz compared with that of PAMAM-G4-$[Gd(DO3A\text{-}MA)(H_2O)]_{31}$, where Gd^{3+} is complexed in DO3A-MA macrocyclic units. Similarly high relaxivities are observed for the HB dendrimers HB-PEI-$[Gd(DOTA\text{-}p\text{Bn})(H_2O)]^-_{32}$ and HB-PG-$[Gd(DOTA\text{-}p\text{Bn})(H_2O)]^-_{68}$ which also bear DOTA chelating units (Fig. 2, panels c, d). Analogous results were reported separately by Bryant et al. [8] for DOTA-type and by Margerum et al. [9] for DO3A-MA type PAMAM dendrimers, however the reasons for the relaxivity difference have not been addressed so far.

Table 2 Parameters obtained for various $GdL(H_2O)^{n-}$ complexes from the simultaneous fitting of ^{17}O NMR and ^{1}H NMR dispersion (*NMRD*) data

Ligand (L)	$(DOTA\text{-}p\text{Bn-}NH_2)^{4-}$	$(DO3A\text{-}AEM)^{3-}$	$DOTA^{4-}$ [a]	$(DO3A\text{-}p\text{Bn-}NO_2)^{3-}$ [b]
k_{ex}^{298} (10^6 s^{-1})	6.6 ± 0.4	3.4 ± 0.3	4.6	1.6
$\Delta H^{\ddagger}$ (kJ mol^{-1})	50.1 ± 1.0	44.8 ± 1.3	54.5	40.9
$\Delta S^{\ddagger}$ (J mol^{-1} K^{-1})	53.7 ± 0.3	30.1 ± 0.6	65	11.1
$A/\hbar$ (10^6 rad s^{-1})	–3.6 ± 0.1	–3.7 ± 0.3	–4.0	–3.8
τ_{rO}^{298} (ps)	199 ± 3	180 ± 7	100	210
E_R (kJ mol^{-1})	20.7 ± 0.5	16.0 ± 1.4	20.0	17.7

[a] From [44]

[b] From [10]

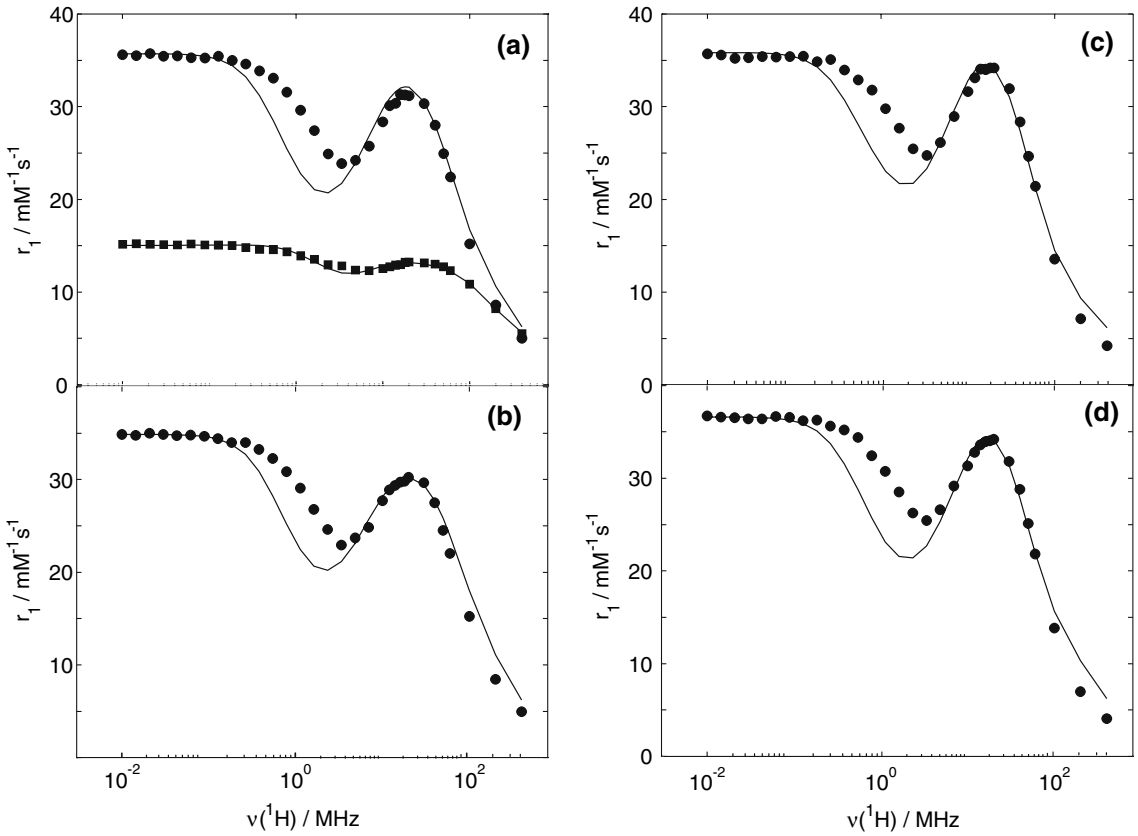

Fig. 2 ^{1}H NMRD profiles of PAMAM-G4-[Gd(DOTA-*p*Bn)$(H_2O)]^{-}_{33}$ (*circles*) and PAMAM-G4-[Gd(DO3A-MA)$(H_2O)]_{31}$ (*squares*) (*a*), PAMAM-G4-PEG-[Gd(DOTA-*p*Bn)$(H_2O)]^{-}_{38}$ (*b*), HB- PEI-[Gd(DOTA-*p*Bn)$(H_2O)]^{-}_{32}$ (*c*), and HB-PG-[Gd(DOTA-*p*Bn)$(H_2O)]^{-}_{68}$ (*d*) at 298 K

We analyzed the proton relaxivities using the Solomon–Bloembergen–Morgan equations including the Lipari–Szabo approach (equations in the electronic supplementary material). This model has been successfully used to analyze ^{17}O and ^{1}H NMR relaxation data with respect to rotational dynamics of various macromolecules [39, 40], including dendrimers [41, 42]. The Lipari–Szabo approach describes the rotational dynamics in macromolecules with two correlation times referring to two statistically independent processes: (1) a rapid local motion of the Gd^{3+} chelates on the dendrimeric surface (τ_1) and (2) a slow global motion of the entire molecule (τ_g). The model also involves a general order parameter, S^2, related to the degree of spatial restriction of the local motion with respect to the global one. When $S^2 = 0$, the internal motion is totally free, whereas for $S^2 = 1$ the rotational dynamics is determined only by the global motion.

Although ^{1}H NMRD curves were recorded at two temperatures, only those at 298 K were analyzed

because the relaxivity changes only slightly between 310 and 298 K. A maximum in relaxivity is observed at 40 MHz at about 298 K (Fig. 3), pointing towards a limitation of relaxivity by slow exchange at lower temperatures. According to previous studies, covalent attachment of Gd^{3+} chelates to macromolecules does not significantly affect the rate and mechanism of water exchange [10, 41, 42]; therefore, in the analysis of the proton relaxivities of the dendrimers, water exchange rates determined for the corresponding monomeric complexes, $[Gd(DOTA\text{-}p\text{Bn-}NH_2)(H_2O)]^-$ and [Gd (DO3A-AEM)(H_2O)], were used. Similarly, the number of inner-sphere water molecules (q) was also fixed to one for each dendrimer. The experimental NMRD data and the fitted curves for the PAMAM and HB dendrimers studied are shown in Fig. 2, and the parameters obtained in the fit are given in Table 3.

The global and local rotational correlation times obtained from the ^1H longitudinal relaxation rates are the most relevant parameters of the analysis. Because of the shortcomings of the Solomon–Bloembergen–Morgan theory, there is in general a deviation between calculated and measured proton relaxivities around the minima of the NMRD curves (0.2–5 MHz) [33]. A data analysis using a more rigorous theoretical description of electron spin relaxation for slowly rotating molecules would imply a variable-temperature and variable-field NMR relaxation as well as the necessity of EPR study, which is beyond the scope of this work. Furthermore, the Lipari–Szabo approach has not been implemented in the slow-motion theories developed so far [31]. The longitudinal electron spin relaxation, $1/T_{1e}$, decreases with increasing Larmor frequency and

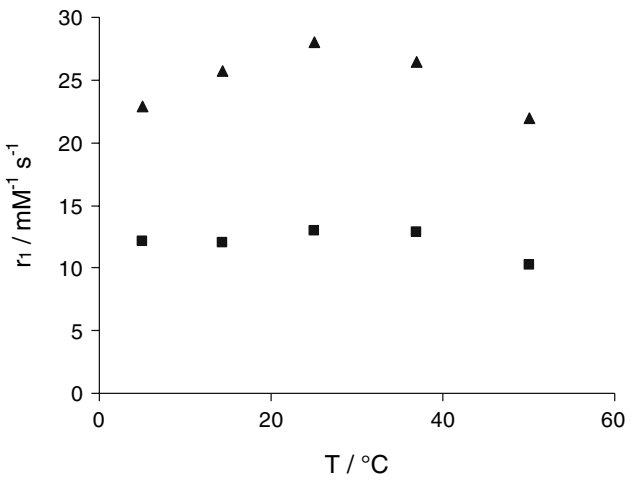

Fig. 3 Temperature-dependent relaxivities for PAMAM-G4-$[Gd(DOTA\text{-}p\text{Bn})(H_2O)]_{33}^-$ (*circles*) and PAMAM-G4-[Gd (DO3A-MA)(H_2O)]$_{31}$ (*squares*) at 40 MHz

becomes small compared to the speed of rotational motion, which is constant. The global and local correlation times τ_g and τ_l, respectively, are therefore reasonably well determined by relaxivities at high magnetic fields. Relaxivities at low frequencies are—as for monomeric complexes—described by effective electron spin relaxation parameters which are not very different from those obtained for the fast-rotating complexes (Tables S5, S11).

As Table 3 shows, rotational motion of PAMAM-G4-$[Gd(DO3A\text{-}MA)(H_2O)]_{31}$, expressed by τ_g and τ_l, is much faster than for all the other dendrimers containing a DOTA-type chelating unit. Similarly, the order parameter S^2 is also the smallest for the dendrimer with the DO3A-MA chelating unit, indicating a considerable internal flexibility. This faster rotation found for PAMAM-G4-$[Gd(DO3A\text{-}MA)(H_2O)]_{31}$ is mainly responsible for its lower relaxivity. The difference in the rotational dynamics of these dendrimers is likely related to their different charges: in contrast to the neutral Gd^{3+}-DO3A-MA, the $[Gd(DOTA\text{-}p\text{Bn-}NH_2)(H_2O)]^-$ chelates represent an important negative charge on the surface of the dendrimer. The repulsion between these negative charges probably leads to more rigidity on the surface, and also to an increased overall size of the macromolecule. It has to be noted, however, that the exact overall charge of the dendrimer complexes is very difficult to define. First, the loading of the dendrimers with the macrocyclic ligand is between 60 and 70% with respect to the overall number of terminal amines; thus, there are free amine groups on the dendrimer surface. Furthermore, not all macrocyclic chelators are complexed with Gd^{3+}. One can say nevertheless that the dendrimers loaded with $Gd(DOTA)^-$ will have a more negative charge than their analogues bearing Gd(DO3A)-MA units. Recently, we showed that charge effects can be very important in determining the rotational dynamics of dendrimeric Gd^{3+} complexes [41]. The protonation of the internal amine nitrogens in a Gd^{3+}-loaded PAMAM dendrimer results in an increased repulsion between the positive charges and leads to an increased size and thus to a slower global motion of the macromolecule. This is manifested in strongly pH dependent relaxivities, increasing with decreasing pH. Another parameter that can also contribute to the different rotational dynamics of the dendrimers loaded with $Gd(DOTA)^-$ or Gd(DO3A)-MA is the nature (flexibility, length) of the spacer that is used to connect the Gd^{3+} complex to the macromolecular scaffold. This effect is most obvious in the large difference of the τ_l^{298} values, which are much higher for the $Gd(DOTA)^-$-containing dendrimers than for PAMAM-G4-$[Gd(DO3A\text{-}MA)(H_2O)]_{31}$.

Table 3 Parameters obtained for the macromolecular Gd^{3+} complexes by fitting the ^1H NMRD data with the use of the Lipari–Szabo approach

Dendrimers	k_{298}^{ex} (10^6 s^{-1})	τ_g^{298} (ps)	τ_l^{298} (ps)	S^2
PAMAM-G4-[Gd(DOTA-*p*Bn)$(H_2O)]^-_{33}$	6.6[a]	3,100 ± 900	550 ± 200	0.39 ± 0.14
PAMAM-G4-[Gd(DO3A-MA)$(H_2O)]_{31}$	3.4[a]	970 ± 100	140 ± 20	0.33 ± 0.05
PAMAM-G4-PEG-[Gd(DOTA-*p*Bn)$(H_2O)]^-_{38}$ [a]	6.6[a]	2,400 ± 200	620 ± 140	0.43 ± 0.06
HB-PEI-[Gd(DOTA-*p*Bn)$(H_2O)]^-_{32}$	6.6[a]	3,800 ± 300	390 ± 110	0.39 ± 0.05
HB-PG-[Gd(DOTA-*p*Bn)$(H_2O)]^-_{68}$	6.6[a]	4,000 ± 400	530 ± 120	0.36 ± 0.05

[a] The value was fixed in the fit

In addition to the different rotational dynamics, a slower electron spin relaxation of the DOTA-loaded dendrimers compared with the DO3A amide loaded dendrimers can also contribute to the different proton relaxivities, particularly at low field. As a third factor, the slight difference in the water exchange rate of $Gd(DOTA)^-$ and GdDO3A-MA chelates has also to be considered. However, the different water exchange rate contributes only to a very limited extent to the proton relaxivity difference at 298 K. We simulated a NMRD curve by using the parameters calculated for PAMAM-G4-[Gd(DO3A-MA)$(H_2O)]_{31}$, except for the water exchange rate, which was fixed to the value obtained for [Gd(DOTA-*p*Bn-NH_2)$(H_2O)]^-$, k_{ex} = 6.6×10^6 s^{-1}, instead of $k_{ex} = 3.4 \times 10^6$ s^{-1} determined for [Gd(DO3A-AEM)(H_2O)]. The faster water exchange rate results in only 10–20% higher relaxivities, and can in no way explain the experimentally observed high r_1 values for the DOTA-loaded dendrimers (see electronic supplementary material). Most likely it is the rotational dynamics—certainly related to the different charge—which is responsible for the large difference in the longitudinal proton relaxivity between the DOTA-loaded and the DO3A amide loaded dendrimers. It is interesting to observe that the order of the relaxivities is reversed at 400 MHz: PAMAM-G4-[Gd(DO3A-MA)$(H_2O)]_{31}$ has the highest value among all dendrimeric complexes (5.66 vs. 4.78 mM^{-1} s^{-1} for PAMAM-G4-[Gd(DOTA-*p*Bn)$(H_2O)]^-_{33}$, 4.68 mM^{-1} s^{-1} for PAMAM-G4-PEG-[Gd(DOTA-*p*Bn)$(H_2O)]^-_{38}$, 3.88 mM^{-1} s^{-1} for HB-PEI-[Gd(DOTA-*p*Bn)$(H_2O)]^-_{32}$, and 3.76 mM^{-1} s^{-1} for HB-PG-[Gd(DOTA-*p*Bn)$(H_2O)]^-_{68}$, at 310 K). This is in full accordance with the expectations: the Solomon–Bloembergen–Morgan theory predicts that at frequencies above 200 MHz the relaxivity increases with the inverse rotational correlation time, while at lower frequencies, it is proportional to τ_R. It implies that at high fields molecules with ''intermediate'' slow rotation such as PAMAM-G4-[Gd(DO3A-MA)$(H_2O)]_{31}$ are favorable over more slowly rotating ones. This theoretically predicted effect is nicely reflected in the observed order of the 400-MHz relaxivities of the dendrimers studied here.

The modification of the dendrimer surface with PEG chains (PAMAM-G4-PEG-[Gd(DOTA-*p*Bn)$(H_2O)]^-_{38}$) is expected to result in much longer blood circulation time. As far as the relaxivity values are concerned, there is no detectable effect of the PEGylation. According to our analysis, the rotational dynamics of the dendrimer is not significantly influenced by the presence of the PEG chains (Table 4). This is also in good agreement with the observation of Margerum et al. [9].

The PEI- and PG-based HB dendrimers (HB-PEI-[Gd(DOTA-*p*Bn)$(H_2O)]^-_{32}$, HB-PG-[Gd(DOTA-*p*Bn)$(H_2O)]^-_{68}$) have relaxivities comparable to or slightly higher than those of the PAMAM dendrimers (Fig. 4), which is reflected in a similar rotational dynamics behavior; therefore, one can conclude that, in terms of relaxation efficiency, HB structures represent as good macromolecular scaffolds as regular dendrimers for MRI CA applications. Given their much easier synthesis, their use may become more important in the future.

MRI studies in vivo

The CA was very well tolerated by the mice. No gross side effects during injection or after the experiment were observed. MRI was performed with all the different dendrimers and in general the resulting CA properties such as vascular circulation time, leakiness in the tumor tissue, and excretion via the kidneys were marginally different, with the exception of the extended blood half life of the PEGylated dendrimer. At the field of the imaging (4.7 T), almost identical in vitro relaxivities were measured for all the dendrimers (Fig. 2). The in vivo studies also showed very similar efficiency for all of them.

Images of the in vivo experiment with PAMAM-G4-PEG-[Gd(DOTA-*p*Bn)$(H_2O)]^-_{38}$ in one mouse are displayed in Fig. 4: Fig. 4a and b shows coronal IR FLASH images of the lower abdomen before and

Table 4 Comparison of longitudinal proton relaxivities at 20 MHz for different Gd^{3+}-loaded dendrimers

Dendrimers	T (K)	R_1 (mM^{-1} s^{-1}) (20 MHz)	Molecular mass (kg mol^{-1})	References
PAMAM-G4-[Gd(DOTA-*p*Bn)(H_2O)]$^{-}_{33}$	298	31.2	45	This work
PAMAM-G4-[Gd(DO3A-MA)(H_2O)]$_{31}$	298	13.2	35	This work
PAMAM-G4-PEG-[Gd(DOTA-*p*Bn)(H_2O)]$^{-}_{38}$[a]	298	30.2	60	This work
HB- PEI-[Gd(DOTA-*p*Bn)(H_2O)]$^{-}_{32}$	298	34.2	50	This work
HB-PG-[Gd(DOTA-*p*Bn)(H_2O)]$^{-}_{68}$	298	34.2	95	This work
G5((N{CS}-Bn-Gd-(DOTA)(H_2O))$^{-}_{96}$	296	30	118	[8]
G4((N{CS}N-Bn-Gd-(DO3A-MA)(H_2O))$_{38}$	310	16.9	37	[9]
Gadomer 17	298	16.5	18	[40]
G6((N{CS}-Bn-Gd-(DTPA)(H_2O))$^{2-}_{170}$	293	34[a]	139	[7]
G5-(GdEPTPA)(H_2O)$^{2-}_{111}$	298	25.1	114	[41]

[a] 25 MHz

12 min after CA injection. In the preinjection image, the vena cava, the kidneys, and especially the tumor were dark owing to the choice of the inversion delay. After injection, kidneys and the vena cava became lighter as a result of T_1 shortening, and the tumor showed a relatively smaller enhancement. Figure 4c shows an anatomical RARE image of the axial imaging slice in the same mouse. Again, in the preinjection IR FLASH image (Fig. 4d) signal intensity was low. Immediately after injection (Fig. 4e), the blood in the vena cava and the cortex of the kidney were enhanced. Some seconds later (Fig. 4f), the medulla of the kidney

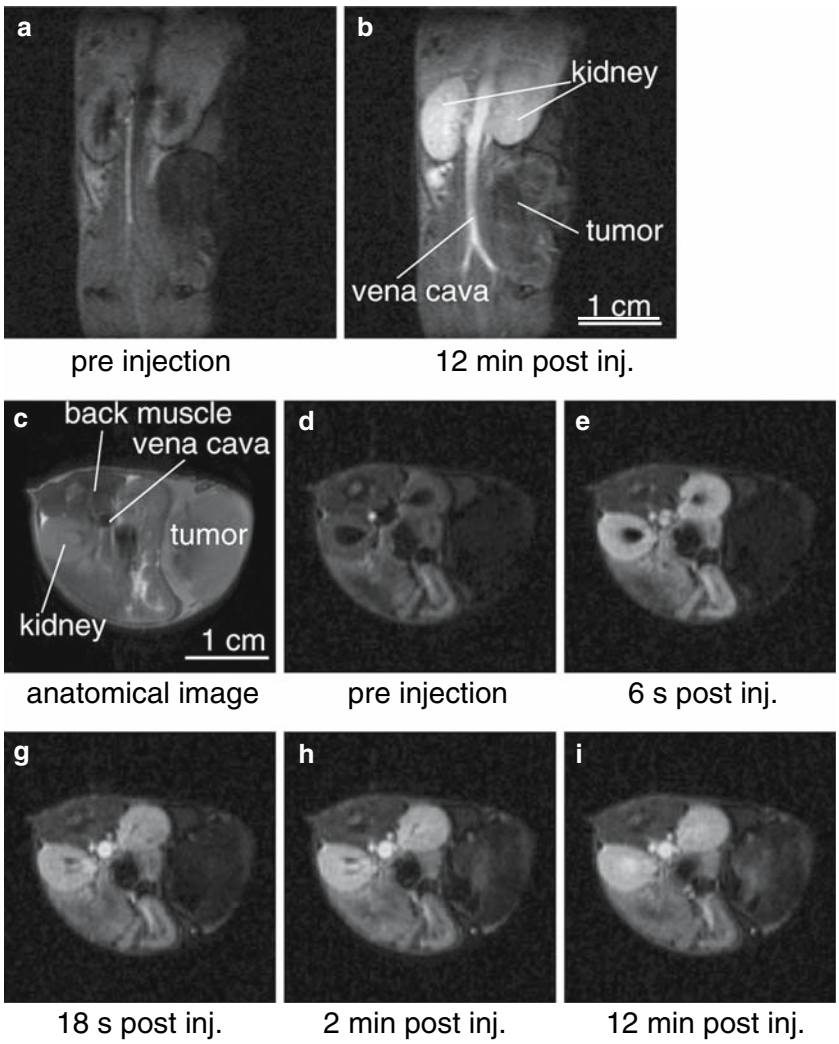

Fig. 4 Inversion-recovery fast low-angle shot (*IR FLASH*) magnetic resonance images before and after intravenous injection of PAMAM-G4-PEG-[Gd(DOTA-*p*Bn)(H_2O)]$^{-}_{38}$ in an in vivo experiment in a mouse bearing a subcutaneous tumor in the lower flank. **a**, **b** Coronal images of the lower abdomen with the kidneys and the tumor at the time point indicated. **c** Anatomical image of the axial imaging slice. **d–h** Axial IR FLASH magnetic resonance images at several time points showing the kidneys, the tumor, and the back (paravertebral) muscle around the spine. The vena cava can be seen between the kidneys

and also some vessels in the skin surrounding the tumor became lighter. Two minutes after injection (Fig. 4g), CA uptake was visible in the tumor core. At the end of the DCE-MRI experiment (Fig. 4h), the cortex of the kidneys and the blood in the vena cava were still bright, and the tumor core and the medulla of the kidney were further enhanced. There was also a small enhancement in the paravertebral muscle and the tumor rim.

The Gd concentration–time curves in Fig. 5 show the kinetics of CA uptake in the different ROIs. The Gd concentration in the blood pool (red curve) did not diminish (the relatively high noise in the curve is due to motion artifacts which had an effect on this small ROI) over 12 min, confirming that PAMAM-G4-PEG-$[Gd(DOTA\text{-}p Bn)(H_2O)]^{-}{}_{38}$ is a blood pool agent. It had a very long half life in blood and a very low leakage to tissue (extracellular, extravascular space) owing to the size of the dendrimer scaffold and owing to the attached PEG chains. The very low leakage was confirmed by the low Gd concentration in the muscle (green curve) and in the tumor rim (orange curve), where the CA remained intravascular. The low Gd concentration reflected the low blood volume in these two tissue types, which is in the same range for both. The delayed and increased CA uptake in the tumor core (light-blue curve) can be explained by the slow diffusion of the CA into this presumably necrotic compartment where the CA accumulated in the extracellular space. The CA is mainly filtered from the blood stream by the kidneys, which can be seen in the high Gd concentration in this organ (gray and dark-blue curves).

In conclusion, all dendrimeric CAs act as blood pool agents suitable for angiography and also for the study of vasculature parameters like blood volume and permeability of, e.g., tumor vessels [43]. Attaching targeting moieties like drugs, peptides, or antibodies to the dendrimers surface will lead to target-specific vascular MRI CAs which can be helpful in early-phase drug testing by small animal imaging. Subsequent studies will show if the stealth properties of PEG chains attached to macromolecular CAs not to be phagocyted are necessary for target-specific imaging by extended blood circulation.

Conclusions

We have reported the synthesis and in vitro and in vivo characterization of a series of PAMAM-G4 dendrimers and, for the first time, HB dendrimeric structures loaded with macrocyclic Gd^{3+} chelates on their surface. The Gd^{3+} was complexed either by the tetraazatetracarboxylate $DOTA^{4-}$ unit (DOTA-$p Bn^{4-}$) or by the tetraazatricarboxylate MA DO3A-MA^{3-} chelator. Approximately twice as high proton relaxivities were found at frequencies below 200 MHz for the dendrimers loaded with the negatively charged Gd(DOTA-$p Bn)^{-}$ in comparison with the dendrimeric complex bearing the neutral Gd(DO3A-MA) moieties. The analysis of the proton relaxivities in terms of local and global rotational motion using the Lipari–Szabo approach allowed us to conclude that it is almost exclusively the different rotational dynamics which is responsible for the different proton relaxivities. The slower rotation of the Gd(DOTA-$p Bn)^{-}$-loaded dendrimers is likely related to a negative charge of the complex which creates more rigidity and increases the overall size of the macromolecule compared with the dendrimer loaded with the neutral Gd(DO3A-MA) complex. PEGylation of the dendrimers does not influence the proton relaxivity. HB dendrimers have been proven to be as good macromolecular scaffolds

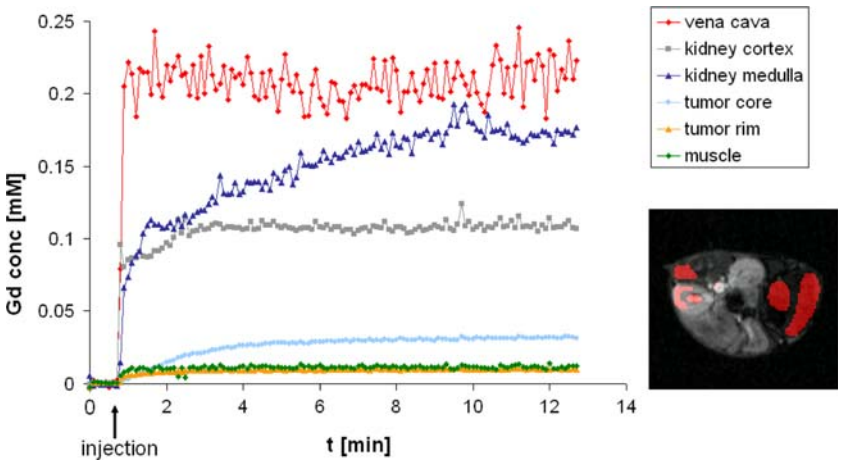

Fig. 5 Mean Gd concentration–time courses in several regions (shown in *red* on the magnetic resonance image *insert*) of the same in vivo experiment as shown in Fig. 4: blood in the vena cava (*red*), kidney cortex (*gray*), kidney medulla (*dark blue*), tumor core (*light blue*), tumor rim (*orange*), and paravertebral muscle (*green*)

for Gd^{3+} complexes with respect to proton relaxivity as the regular PAMAM dendrimers. The in vivo MRI studies performed on tumor-bearing mice at 4.7 T revealed that all the dendrimeric complexes studied act as blood pool agents suitable for angiography and also for the study of vasculature parameters like blood volume and permeability of, e.g., tumor vessels.

Acknowledgements We thank the Swiss National Science Foundation and the Swiss State Secretariat for Education and Research (SER) for financial support. This work was performed in the frame of the EU COST Actions D18 ''Lanthanide chemistry for diagnosis and therapy'' and D38 ''Metal-based systems for molecular imaging applications'' and the European-founded EMIL program (LSCH-2004–503569).

References

1. Edelman RR, Hesselink JR, Zlatkin MB (1996) MRI: clinical magnetic resonance imaging. Saunders, Philadelphia
2. Caravan P, Ellison JJ, McMurry TJ, Lauffer RB (1999) Chem Rev 99:2293
3. Tóth É, Merbach AE (eds) (2001) The chemistry of contrast agents in medical magnetic resonance imaging. Wiley, Chichester
4. Boas U, Heegaard Peter MH (2004) Chem Soc Rev 33:43
5. Stiriba S-E, Frey H, Haag R (2002) Angew Chem Int Ed Engl 41:1329
6. Qiu LY, Bae YH (2006) Pharm Res 23:1
7. Wiener EC, Brechbiel MW, Brothers H, Magin RL, Gansow OA, Tomalia DA, Lauterbur PC (1994) Magn Reson Med 31:1
8. Bryant LH Jr, Brechbiel MW, Wu C, Bulte JWM, Herynek V, Frank JA (1999) J Magn Reson Imaging 9:348
9. Margerum LD, Campion BK, Koo M, Shargill N, Lai J-J, Marumoto A, Sontum PC (1997) J Alloys Compd 249:185
10. Tóth É, Pubanz D, Vauthey S, Helm L, Merbach AE (1996) Chem Eur J 2:1607
11. Konda SD, Aref M, Brechbiel M, Wiener EC (2000) Invest Radiol 35:50
12. Rudovsky J, Hermann P, Botta M, Aime S, Lukes I (2005) Chem Commun 2390
13. Dong Q, Hurst DR, Weinmann HJ, Chenevert TL, Londy FJ, Prince MR (1998) Invest Radiol 33:699
14. Venditto VJ, Regino CAS, Brechbiel MW (2005) Mol Pharm 2:302
15. Esfand R, Tomalia DA (2001) Drug Discov Today 6:427
16. Voit BI (2003) C R Chimie 6:821
17. Fernandes EGR, De Queiroz AAA, Abraham GA, Roman JS (2006) J Mater Sci Mater Med 17:105
18. Lipari G, Szabo A (1982) J Am Chem Soc 104:4546
19. Lipari G, Szabo A (1982) J Am Chem Soc 104:4559
20. Krämer M, Stumbé J-F, Grimm G, Kaufmann B, Krüger U, Weber M, Haag R (2004) ChemBioChem 5:1081
21. Koç F, Wyszogrodzka M, Eilbracht P, Haag R (2005) J Org Chem 70:2021
22. Ammann C, Meier P, Merbach AE (1982) J Magn Reson 46:319
23. Hugi AD, Helm L, Merbach AE (1985) Helv Chim Acta 68:508
24. Yerly F (1999) Visualiseur 2.3.4. Institute of Molecular and Biological Chemistry, University of Lausanne, Lausanne
25. Yerly F (1999) Optimiseur 2.3.4. Institute of Molecular and Biological Chemistry, University of Lausanne, Lausanne
26. Haase A, Matthaei D, Bartkowski R, Duhmke E, Leibfritz D (1989) J Comput Assist Tomogr 13:1036
27. Jivan A, Horsfield MA, Moody AR, Cherryman GR (1997) J Magn Reson 127:65
28. Kobayashi H, Kawamoto S, Saga T, Sato N, Hiraga A, Ishimori T, Konishi J, Togashi K, Brechbiel MW (2001) Magn Res Med 46:781
29. Tóth É, Helm L, Merbach AE (2001) In: Tóth É, Merbach AE (eds) The chemistry of contrast agents in medical magnetic resonance imaging. Wiley, Chichester, pp 45–120
30. Kowalewski J, Kruk D, Parigi G (2005) Adv Inorg Chem 57:42
31. Helm L (2006) Prog NMR Spectrosc 49:45
32. Belorizky E, Fries PH (2004) Phys Chem Chem Phys 6:2341
33. Helm L, Tóth É, Merbach AE (2003) In: Sigel A, Sigel H (eds) Metal ions in biological systems, vol 40. Marcel Dekker, New York
34. Laurent S, Houzé S, Guérit N, Muller RN (2000) Helv Chim Acta 83:394
35. Vander Elst L, Maton F, Laurent S, Seghi F, Chapelle F, Muller RN (1997) Magn Reson Med 38:604
36. Laurent S, Botteman F, Vander Elst L, Muller RN (2004) Eur J Inorg Chem 3:463
37. Woods M, Kovacs Z, Zhang S, Sherry AD (2003) Angew Chem Int Ed Engl 42:5889
38. Laus S, Ruloff R, Tóth É, Merbach AE (2003) Chem Eur J 9:3555
39. Tóth É, Helm L, Kellar KE, Merbach AE (1999) Chem Eur J 5:1202
40. Nicolle GM, Tóth É, Eisenwiener KP, Mäcke HR, Merbach AE (2002) J Biol Inorg Chem 7:757
41. Laus S, Sour A, Ruloff R, Tóth É, Merbach AE (2005) Chem Eur J 11:3064
42. Nicolle GM, Tóth É, Schmitt-Willich H, Radüchel B, Merbach AE (2002) Chem Eur J 8:1040
43. Leach MO, Brindle KM, Evelhoch JL, Griffiths JR, Horsman MR, Jackson A, Jayson GC, Judson IR, Knopp MV, Maxwell RJ, McIntyre D, Padhani AR, Price P, Rathbone R, Rustin GJ, Tofts PS, Tozer GM, Vennart W, Waterton JC, Williams SR, Workman P (2005) Br J Cancer 92:1599
44. Burai L, Tóth É, Bazin H, Benmelouka M, Jászberényi Z, Merbach AE (2006) Dalton Trans 629